Electrical detection of the surface spin polarization of the candidate topological Kondo insulator SmB_6

Jehyun Kim,[1] Chaun Jang,[2] Xiangfeng Wang,[3] Johnpierre Paglione,[3] Seokmin Hong,[2] Jekwan Lee,[4] Hyunyong Choi,[4] and Dohun Kim[1,*]

[1]*Department of Physics and Astronomy and Institute of Applied Physics, Seoul National University, Seoul 08826, Korea*
[2]*Center for Spintronics, Korea Institute of Science and Technology, Seoul 02792, Korea*
[3]*Center for Nanophysics and Advanced Materials, Department of Physics, University of Maryland, College Park, Maryland 20742-4111, USA*
[4]*School of Electrical and Electronic Engineering, Yonsei University, Seoul 03722, Korea*

(Received 9 December 2018; published 26 June 2019)

The Kondo insulator compound SmB_6 has emerged as a strong candidate for the realization of a topologically nontrivial state in a strongly correlated system, a topological Kondo insulator, which can be a novel platform for investigating the interplay between nontrivial topology and emergent correlation-driven phenomena in solid-state systems. Electronic transport measurements on this material, however, so far showed only the robust surface-dominated charge conduction at low temperatures, lacking evidence of its connection to the topological nature by showing, for example, spin polarization due to spin-momentum locking. Here, we find evidence for surface-state spin polarization by electrical detection of a current-induced spin chemical-potential difference on the surface of a SmB_6 single crystal. We clearly observe that a surface-dominated spin voltage, which is proportional to the projection of the spin polarization onto the contact magnetization, is determined by the direction and magnitude of the charge current and is strongly temperature dependent due to the crossover from surface to bulk conduction. We estimate the lower bound of the surface-state net spin polarization as 25% based on the quantum transport model, providing direct evidence that SmB_6 supports metallic spin helical surface states.

DOI: 10.1103/PhysRevB.99.245148

I. INTRODUCTION

Recent theoretical study identifies SmB_6 as a member of a newly classified family of strong topological insulators, topological Kondo insulators [1–4], in which topologically protected surface states reside in the bulk Kondo band gap at low temperatures due to strong spin-orbit coupling. Following the measurement of the robust surface conduction below several degrees Kelvin [5–7] superimposed with bulk insulating behavior with a *d*–*f* hybridization induced gap in the range of 10–20 meV at intermediate temperatures below 300 K, many experimental efforts have been designed to probe the topological nature of the surface conducting states in this material [8–12].

While the two-dimensional nature of the surface band and surface spin polarization has been confirmed by surface-sensitive probes such as photoemission [11,13] and, most recently, the magnetic resonance induced spin pumping technique showed the possibility to inject a nonequilibrium spin current into the surface of SmB_6 [12], direct electrical measurement of surface current-induced spin-momentum locking, the unique feature of topological insulators, has not been performed in a simple transport geometry.

II. MATERIALS AND METHODS

A. Material growth

Single crystals of SmB_6 were grown with Al flux, starting from elemental Sm and B with the stoichiometry of 1 to 6 in a ratio of $SmB_6 : Al = 1 : 200–250$. The initial materials were placed in an alumina crucible and loaded in a tube furnace under Ar atmosphere. The assembly was heated to 1250–1400 °C and maintained at that temperature for 70–120 h, then cooled at $-2\,°C/h$ to 600–900 °C, followed by faster cooling. The SmB_6 samples were put into sodium hydroxide to remove the residual Al flux.

B. Device fabrication

An Al layer of 2 nm was deposited on the polished (100) surface of SmB_6 by using electron-beam evaporation followed by oxidizing on a hotplate in ambient conditions (see Supplemental Material Figs. S7 and S8 [14]). The resulting thin Al oxide layer prevents direct contact of the ferromagnetic electrode with SmB_6. Standard electron-beam lithography was used to make electrode patterns. A permalloy (Py) layer was used as a ferromagnetic detector for spin chemical-potential measurement, with the lateral size of $150 \times 150\,\mu m^2$ and thickness of 20 nm deposited and capped with 15 nm of Au using electron-beam evaporation. Nonferromagnetic contacts used for the source, drain, and reference electrodes were formed by electron-beam lithography patterning and Al oxide

*Corresponding author: dohunkim@snu.ac.kr

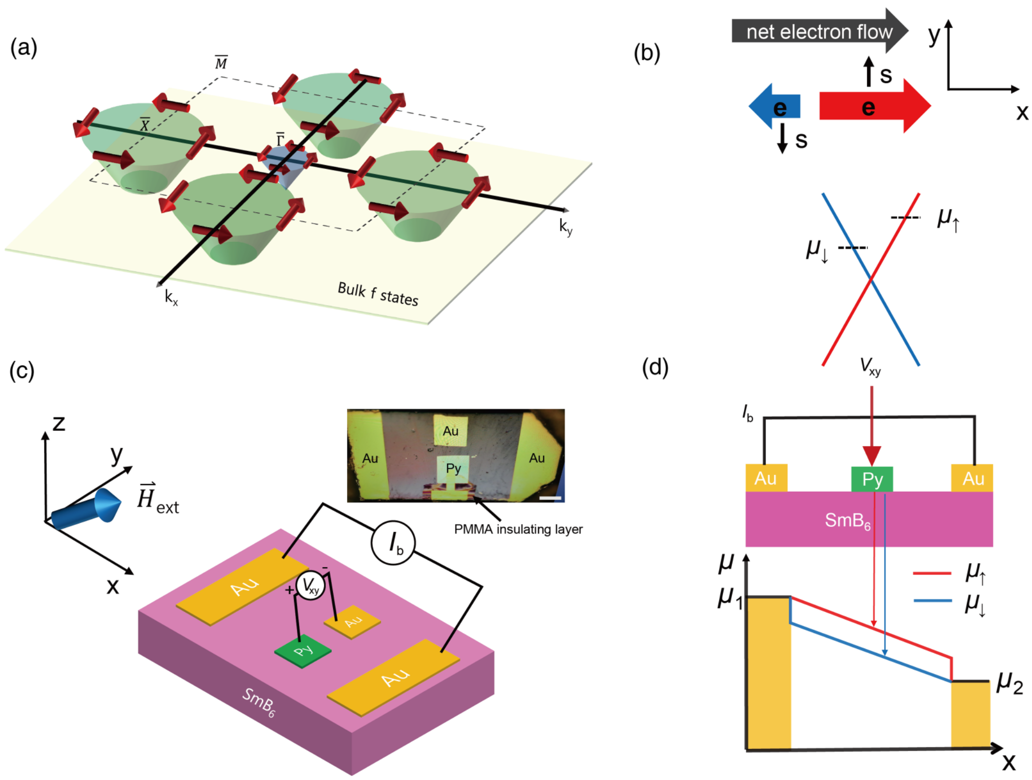

FIG. 1. Surface spin texture and potentiometric spin measurement in SmB_6. (a) Anticlockwise spin texture for the surface band in SmB_6 near the Fermi energy shown by spin and angle-resolved photoemission spectroscopy and first-principles calculations [2,11]. (b) Degree of electron occupation in channel and spin dependent electrochemical potential under electrochemical bias. The length of the red and blue arrows indicates the degree of moving electrons with spin $\boldsymbol{S}$. (c) Measurement configuration for detecting spin voltage. Inset: Optical microscope image of the device. The scale bar is 100 μm. (d) Electrochemical potential with respect to the position of the channel, illustrating concepts of the potentiometric spin measurement.

etching with a buffered oxide etchant followed by depositing Ti 5 nm/Au 80 nm using electron-beam evaporation. For the Au electrode acting as the wire bonding pad for the ferromagnetic contact, an additional insulating layer was made below the metal layer by an overdosing electron beam on an electron-beam resist (PMMA 950A6) with a dose of 10 000 $\mu C/cm^2$ [see the inset to Fig. 1(c)].

C. Transport measurements

The device was placed in a Quantum Design PPMS variable-temperature cryostat for low-temperature electrical measurements. For current-induced spin-polarization measurement, both dc- and ac-type four-point probe measurements were performed. A dc (ac) current was applied through the SmB_6 surface channel from the nonmagnetic contact source to drain using Keithley 2400 (Keithley 6221) instruments, and a Keithley 2182 nanovoltmeter (Stanford Research Systems SR830 Lock-in amplifier) was used for detecting a voltage difference between the Py and reference Au contact.

III. RESULTS

A. Principle of potentiometric spin measurement

Figure 1(a) shows the simplified spin-momentum relation in SmB_6 near the Fermi energy revealed by recent photoemission studies [11] for both $\bar{X}$ and $\bar{\Gamma}$ high-symmetry points. When the electrons are placed under an electrochemical-potential difference, for example, in the x direction, the electrons moving to the right (red arrow) have higher occupation than the electrons moving to the left (blue arrow), which leads to a difference between the electrochemical potentials for spin up $\mu_\uparrow$ and down $\mu_\downarrow$. This momentum asymmetry leads to a spin-polarized current in the y direction due to spin-momentum locking, thus the presence of the spin-momentum locking property in the SmB_6 surface state can be shown electrically by detecting the spin-polarized current generated by the electrochemical-potential difference. We note that the surface bands in SmB_6 exhibit a spin-momentum relation, hence the sign of the expected spin voltage [15–17], opposite to other topological insulators like Bi_2Se_3 [4,18], as we discuss below.

Here, we use a specially designed potentiometric geometry, as shown in Fig. 1(c), to probe the aforementioned spin dependent chemical-potential difference induced by momentum imbalance. A bias current flows through a nonmagnetic contact on the SmB_6 surface with the (100) crystallographic plane in the x direction, and the transverse voltage V_{xy} is measured between a permalloy magnetic contact (Py) and a reference nonmagnetic contact. Figure 1(d) shows the electrochemical potential for spin-up $\mu_\uparrow$ and -down electrons $\mu_\downarrow$ as a function of the SmB_6 channel position. The ferromagnetic contact can detect spin dependent electrochemical potentials according to its magnetization direction, and the spin voltage

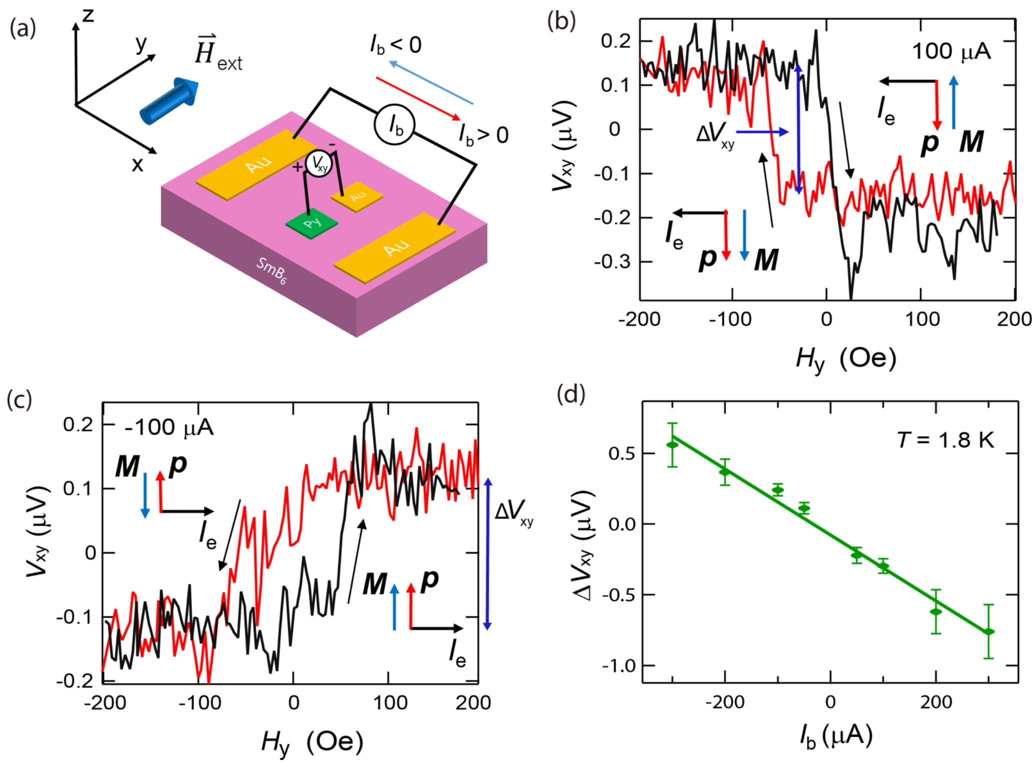

FIG. 2. Measurement of current-induced surface channel spin polarization. (a) Schematic of the transport measurements. A constant current I_b is applied in the x direction while sweeping a magnetic field in the y direction, which is orthogonal to the bias current direction (colinear with the spin-polarization direction). (b, c) Magnetic field dependence of the voltage measured at the ferromagnetic contact for I_b of (b) $+100\,\mu$A and (c) $-100\,\mu$A. Inset: Black, red, and blue arrows indicate the direction of the electron momentum $\boldsymbol{I}_e$, $\boldsymbol{p}$, and $\boldsymbol{M}$, respectively. (d) Dependence of spin voltage ΔV_{xy} on I_b measured at 1.8 K.

corresponding to the difference between the electrochemical potentials for spin up and down can be expressed as follows, based on the quantum transport model [19,20]:

$$\Delta V_{xy} = V_{xy}(\boldsymbol{M}) - V_{xy}(-\boldsymbol{M}) = |I_b| R_B P_{FM} (\boldsymbol{p} \cdot \boldsymbol{M}_{\mathbf{u}}), \qquad (1)$$

where ΔV_{xy} is the spin voltage defined as the difference of the measured electrochemical potential V_{xy} between the opposite detector magnetization $\boldsymbol{M}$ controlled by the external magnetic field $\vec{H}_{ext}$, and ΔV_{xy} is proportional to the magnitude of the bias current $|I_b|$, ballistic resistance of the channel R_B, spin polarization of the ferromagnetic detector P_{FM}, and inner product between the spin polarization of the topological insulator surface $\boldsymbol{p}$ and unit vector $\boldsymbol{M}_u$ along the magnetization of the ferromagnetic detector. As Eq. (1) indicates, we measure ΔV_{xy} as a function of the experimental parameters such as the direction and magnitude of I_b, $\boldsymbol{M}$, and temperature T and confirm the current-induced spin polarization on the surface of SmB_6.

B. Measurement of the current-induced spin polarization

We first show that an electrochemical-potential bias can induce a spin polarization that is reflected in a nonzero ΔV_{xy} measured by the magnetic detector. As shown in Fig. 2(a), V_{xy} is measured by sweeping an external magnetic field in the y axis H_y to control the detector magnetization direction while applying I_b along the x axis. Figures 2(b) and 2(c) show representative spin voltage data recorded with I_b of $+100$ and $-100\,\mu$A, respectively. As the current is applied in the $+x$ ($-x$) direction, where the momenta of the electrons are in the $-x$ ($+x$) direction, the direction of the current-induced spin polarization is parallel to the $-y$ ($+y$) axis due to the anticlockwise spin texture [see the insets of Figs. 2(b) and 2(c) for the detailed directions of the electron momentum $\boldsymbol{I}_e$, $\boldsymbol{p}$, and $\boldsymbol{M}$]. In both Figs. 2(b) and 2(c), a high (low) voltage is measured when the $\boldsymbol{M}$ of the ferromagnet is parallel (antiparallel) to $\boldsymbol{p}$ [15,21] (see Supplemental Material Fig. S1 [14] and Ref. [17]), consistent with the spin-momentum relation in SmB_6 [2,4]. The measured voltage switches near the coercive field of Py (see Supplemental Material Fig. S2 [14] and Refs. [22,23]), which can be explained by the fact that the sign of $\boldsymbol{p} \cdot \boldsymbol{M}_{\mathbf{u}}$ in Eq. (1) changes when the direction of the magnetization is switched. Moreover, the polarity of the hysteresis loop in Figs. 2(b) and 2(c) is the opposite, reflecting the fact that the current-induced spin-polarization direction is dependent on the direction of I_b. More specifically, the measured ΔV_{xy}, which is a difference between V_{xy} ($\boldsymbol{M}$//y axis) and V_{xy} ($\boldsymbol{M}$//-y axis), is shown in Fig. 2(d) as a function of I_b and exhibits a clearly linear response. Therefore, the measured ferromagnetic spin voltage as a function of the magnitude and direction of $\boldsymbol{M}$ and I_b strongly indicates electrical measurement of the current-induced spin polarization on the surface of SmB_6. Additionally, we find spin-to-charge conversion in the SmB_6 surface state through a reciprocal geometry measurement consistent with the Onsager reciprocal relation (see Supplemental Material Fig. S3 [14]

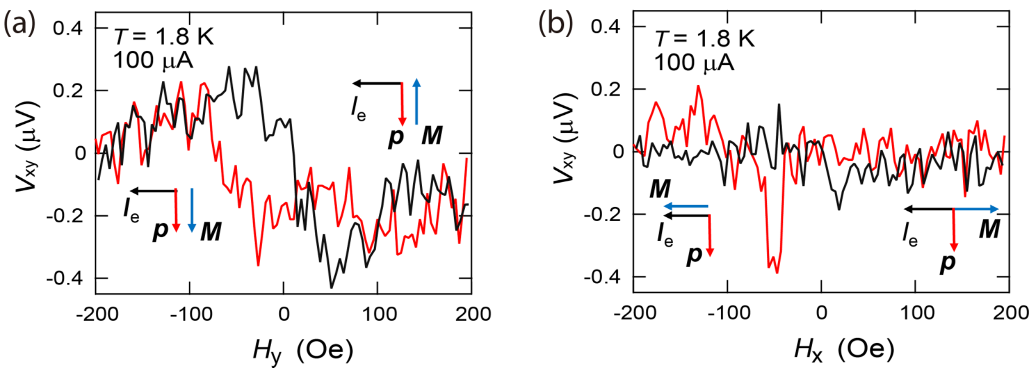

FIG. 3. Magnetization orientation dependence of spin voltage. (a, b) V_{xy} as a function of an external magnetic field swept (a) in the *y* direction and (b) in the *x* direction under I_b of 100 μA at 1.8 K. Inset: Black, red, and blue arrows show the direction of the electron momentum $\boldsymbol{I}_e$, $\boldsymbol{p}$, and $\boldsymbol{M}$, respectively. Detector magnetization $\boldsymbol{M}$ is aligned (a) in the *y* direction (perpendicular to current) and (b) in the *x* direction (parallel to current).

and Refs. [20,24]). In Supplemental Material Fig. S4 [14] and Refs. [17,25,26], we further discuss the degradation of ΔV_{xy} in the nonlinear transport regime at high $|I_b|$ due to Joule heating and subsequent bulk carrier population [25].

The second equality in Eq. (1) provides a quantitative estimation of the degree of surface ensemble spin polarization $|p|$. We estimate $|p|$, extracted from the slope of $\Delta V_{xy}(I_b)$ dependence [see Fig. 2(d)], as ~25%, based on the following experimental conditions and assumptions: $1/R_B$ is given by q^2/h times the number of modes $k_F W/\pi$, where $W = 500\,\mu$m is the width of the current channel and the total Fermi wave number $k_F(0.67\,\text{Å}^{-1})$ [13] can be determined as $k_{F\alpha} + 2k_{F\beta}$, where $k_{F\alpha}$ and $k_{F\beta}$ are the Fermi wave numbers of the α and β bands in the first Brillouin zone, respectively, and the P_{FM} of Py at low temperatures is 0.38 [27]. We note that this is a conservative estimation of $|\boldsymbol{p}|$ since we assume 100% single-surface-dominated conduction, as well as perfect operation of ferromagnetic detector. The inclusion of experimental imperfections, such as the current path through not only the top but also the bottom surface [6], possible (although small) current leakage through the bulk, or imperfect detection efficiency of the ferromagnetic detector, will only make the estimation of $|\boldsymbol{p}|$ higher, so that our estimation sets the lower bound of the surface current-induced ensemble spin polarization of SmB_6.

C. Exclusion of possible artifacts

To further confirm the origin of V_{xy}, in particular, to exclude the possibility that the hysteresis loops of V_{xy} in Fig. 2 could be due to spurious effects such as the planar Hall effect from the fringe field of the ferromagnetic detector [28], we perform a control experiment by applying $\vec{H}_{ext}$ in the *x* direction, where $\boldsymbol{M}$ is orthogonal to $\boldsymbol{p}$. Figures 3(a) and 3(b) show the results of the V_{xy} when applying $\vec{H}_{ext}$ in the *y* direction and *x* direction, respectively, and the insets show the direction of $\boldsymbol{I}_e$, $\boldsymbol{p}$, and $\boldsymbol{M}$ like that shown in Figs. 2(b) and 2(c). Compared to Fig. 3(a), when the magnetic field is swept in the *x* direction, we do not observe the spin chemical-potential difference ΔV_{xy} at high positive or negative H_x, reflecting that the measured ΔV_{xy} clearly follows the current-induced spin-polarization origin, as the $\boldsymbol{p} \cdot \boldsymbol{M_u}$ term in Eq. (1) indicates. The intermittent nonzero signal in Fig. 3(b) likely stems from the magnetic domain, the transient magnetization direction of which has some *y*-axis component. The result shows that the measured ΔV_{xy} depends on the projection of the spin polarization onto the detector magnetization direction consistent with the spin-texture model of SmB_6.

D. Temperature dependence of the spin voltage

We now turn to discussing the surface origin of the measured spin voltage. The potentiometric measurement performed at 1.8 K already shows evidence of spin polarization in the surface-dominated transport regime. We further confirm this by investigating the temperature dependence of ΔV_{xy} with the concurrently measured temperature-dependent charge conduction. As shown in Fig. 4(a), the temperature-dependent electrical resistance R(T) of SmB_6 exhibits thermally activated behavior at intermediate temperatures below 12 K, before saturating at an approximately temperature-independent value below several degrees Kelvin, typically 4 K, strongly supporting the model of the insulating bulk with metallic surface states, as previously probed by other techniques [5,7]. Performed at temperatures ranging from 1.8 to 4.5 K [marked by red dots in Fig. 4(a)], Figs. 4(b)–4(g) show V_{xy} as a function of H_y under $|I_b|$ of 100 μA. Strong temperature dependence is observed with vanishing ΔV_{xy} at ~4 K, which closely follows the crossover from surface- to bulk-dominated charge conduction around the same temperature [see the inset to Fig. 4(a)]. Moreover, when we consider two parallel channels combined with surface channel resistance independent of temperature and bulk channel resistance dependent on temperature, the ratio between current flowing through the surface channel at different temperatures is determined by the ratio between total resistance at different temperatures. From 1.8 to 4 K, the overall resistance is reduced by 60%, while ΔV_{xy} nearly completely vanishes, which indicates that the additional spin-polarization reduction such as spin-flip scattering between the surface and bulk conduction channels or spin current cancellation between opposite spin polarizations of the surface and bulk spin Hall effect may be important to understand net spin polarization at elevated temperatures. Overall, the results not only confirm that the measured ΔV_{xy} indeed originates from a surface-dominant effect but also show that bulk SmB_6 does not exhibit spin-momentum locking.

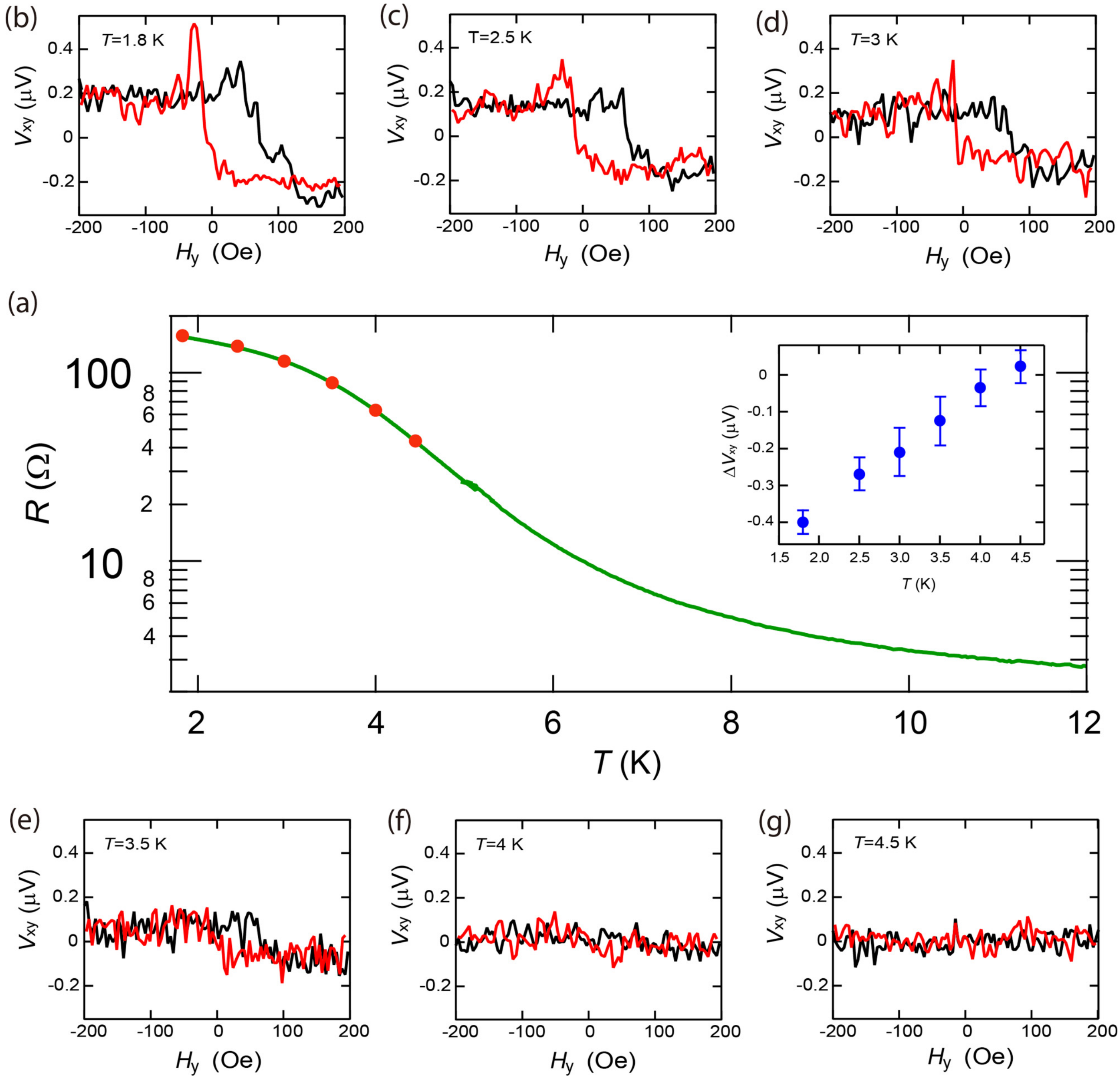

FIG. 4. Temperature dependence of the spin voltage and resistance of SmB_6. (a) Electrical resistance of SmB_6 as a function of temperature. Inset: Spin voltage ΔV_{xy} as a function of temperature. (b–g) V_{xy} measured by sweeping $\overrightarrow{H}_{ext}$ parallel to the y axis under a bias current of 100 μA at different temperatures: (b) 1.8 K, (c) 2.5 K, (d) 3 K, (e) 3.5 K, (f) 4 K, and (g) 4.5 K.

E. Magnetic field angle dependence of the spin voltage

The fact that the surface-dominated ΔV_{xy} shows a clear in-plane anisotropy with respect to the directions of I_b and $\boldsymbol{M}$ provides strong evidence for a spin-momentum locked surface spin polarization in SmB_6. However, the described measurements alone do not distinguish the in-plane vs out-of-plane nature of the spin polarization in SmB_6. We finally discuss this by showing an angle-resolved spin voltage measurement. We apply 2 T of $|\overrightarrow{H}_{ext}|$ to ensure saturation of $\boldsymbol{M}$ to the direction of $\overrightarrow{H}_{ext}$ and rotate the field in the y-z plane as shown in Fig. 5(a), where γ is the angle between the direction of $\boldsymbol{M}$ and the y axis. $|I_b|$ of 300 μA is applied in the $+x$ or $-x$ direction, and γ-dependent V_{xy} is recorded at 2 K. For an accurate spin voltage analysis, the Hall voltage with sin γ dependence (proportional to the z component of an external magnetic field), as well as higher-order magnetoresistance components, were excluded from the raw V_{xy} data (see Supplemental Material Fig. S5 [14] and Refs. [29,30]). Figure 5(b) shows the resulting ΔV_{xy} (γ) in polar coordinates normalized to the maximum spin voltage $\Delta V_{xy,max}$. The vanishing spin voltage in the out-of-plane configuration ($\gamma = 90^\circ$ or 270°), while $\Delta V_{xy,max}$ occurs near $\gamma = 0^\circ$ and 180°, clearly indicates an overall in-plane ensemble spin polarization on the surface of SmB_6 within the experimental error of the field angle calibration of several degrees. We note that the actual angular distribution of ΔV_{xy} in SmB_6 may have a richer structure than a simple cosine function [compare in Fig. 5(b) the data and the fit represented by the solid line], which may stem from the

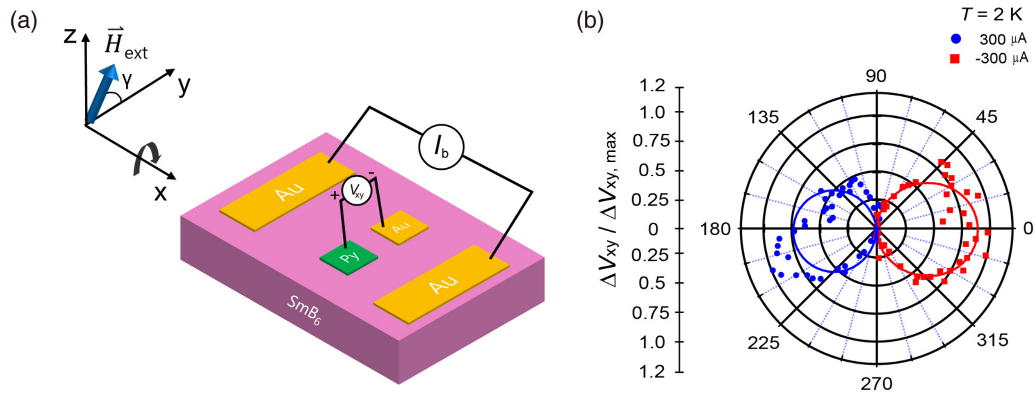

FIG. 5. Angle-resolved current-induced spin polarization. (a) Schematic measurement configuration for potentiometric measurement with rotating magnetic field in the *y-z* plane, where γ is the angle between the applied external magnetic field and the *y* axis. (b) Polar plot of normalized ΔV_{xy} as a function of γ showing the in-plane character of the current-induced spin polarization in SmB_6.

nonatomically flat surface morphology of the polished SmB_6 crystal or, possibly, from the combined effects of multiple conduction surface bands in SmB_6. However, more precise determination of ΔV_{xy} (γ) is not possible with the signal-to-noise ratio of the current experiment, and we leave it for the future work.

IV. DISCUSSION

A simple potentiometric geometry with a ferromagnetic contact enables direct electrical measurement of spin chemical potential in the proposed topological Kondo insulator SmB_6. Unlike the situation in conventional topological insulators like Bi_2Se_3 [31,32], the location of the Fermi energy, pinned near the hybridization-induced gap due to the Kondo mechanism, guarantees surface-dominated transport in SmB_6 at low temperatures, thereby allowing clear surface spin voltage measurement even without extrinsic chemical doping [33] or gating technique [34,35] conventionally used for nonideal topological insulators [32]. The absence of chemical doping or surface gating makes it very likely that the SmB_6 studied here is free from surface band bending related two-dimensional electron gas [36], further confirming that the measured spin voltage mainly stems from the intrinsic surface spin polarization (see Supplemental Material Fig. S9 [14] and Refs. [20,37–39]). However, we do not rule out, although it is estimated to be small [19], the possible contribution from the detailed spin textures of the structural-symmetry-broken Rashba surface states, the spin voltage sign of which cannot be distinguished from the topologically protected surface state in the case of SmB_6, as noted earlier, since, unlike Bi_2Se_3, SmB_6 shows the same anticlockwise spin texture as that of Rashba surface states in most cases [11,19]. Further systematic study on the in-plane magnetization angle dependence or high-resolution spin-resolved photoemission combined with theoretical calculation is needed to fully separate the topologically nontrivial and trivial spin-polarization contributions. Nevertheless, with the ability to clearly measure the intrinsic surface-dominated spin polarization in strongly correlated systems, this approach provides potential for both fundamental and applied spin transport studies in newly proposed topologically nontrivial states of matter.

ACKNOWLEDGMENTS

This research was supported by the Basic Science Research Program (Grants No. NRF-2015R1C1A1A02037430 and No. 2018R1A2A3075438), Priority Research Centers Program (Grant No. 2015R1A5A1037668) through the National Research Foundation of Korea (NRF) funded by the Ministry of Science, ICT and Future Planning, Research Resettlement Fund for the new faculty of Seoul National University, and Creative-Pioneering Researchers Program through Seoul National University. H.C. and J.L. were supported by National Research Foundation of Korea (NRF) through the government of Korea (Grant No. NRF-2018R1A2A1A05079060) and Creative Materials Discovery Program (Grant No. 2017M3D1A1040828). Preparation of SmB_6 material was funded by AFOSR (Grant No. FA9550-14-1-0332) and by the Gordon and Betty Moore Foundations EPiQS Initiative through Grant No. GBMF4419. Electrical measurements used shared facilities funded by the KIST institutional program and the National Research Council of Science and Technology (Grant No. CAP-16-01-KIST).

J.K. and C.J. contributed equally to this work.

[1] M. Dzero, K. Sun, V. Galitski, and P. Coleman, Topological Kondo Insulators, Phys. Rev. Lett. **104**, 106408 (2010).

[2] R. Yu, H. M. Weng, X. Hu, Z. Fang, and X. Dai, Model Hamiltonian for topological Kondo insulator SmB_6, New J. Phys. **17**, 023012 (2015).

[3] T. Takimoto, SmB: A promising candidate for a topological insulator, J. Phys. Soc. Jpn. **80**, 123710 (2011).

[4] R. Yu, H. M. Weng, Z. Fang, and X. Dai, Pseudospin, real spin, and spin polarization of photoemitted electrons, Phys. Rev. B **94**, 085123 (2016).

[5] P. Syers, D. Kim, M. S. Fuhrer, and J. Paglione, Tuning Bulk and Surface Conduction in the Proposed Topological Kondo Insulator SmB_6, Phys. Rev. Lett. **114**, 096601 (2015).
[6] S. Wolgast, Ç. Kurdak, K. Sun, J. W. Allen, D.-J. Kim, and Z. Fisk, Low-temperature surface conduction in the Kondo insulator SmB_6, Phys. Rev. B **88**, 180405(R) (2013).
[7] D. J. Kim, S. Thomas, T. Grant, J. Botimer, Z. Fisk, and J. Xia, Surface hall effect and nonlocal transport in SmB_6: Evidence for surface conduction, Sci. Rep. **3**, 3150 (2013).
[8] M. Neupane *et al.*, Surface electronic structure of the topological Kondo-insulator candidate correlated electron system SmB_6, Nat. Commun. **4**, 2991 (2013).
[9] Y. Nakajima, P. Syers, X. F. Wang, R. X. Wang, and J. Paglione, One-dimensional edge state transport in a topological Kondo insulator, Nat. Phys. **12**, 213 (2016).
[10] D. J. Kim, J. Xia, and Z. Fisk, Topological surface state in the Kondo insulator samarium hexaboride, Nat. Mater. **13**, 466 (2014).
[11] N. Xu *et al.*, Direct observation of the spin texture in SmB_6 as evidence of the topological Kondo insulator, Nat. Commun. **5**, 4566 (2014).
[12] Q. Song *et al.*, Spin injection and inverse Edelstein effect in the surface states of topological Kondo insulator SmB_6, Nat. Commun. **7**, 13485 (2016).
[13] J. Jiang *et al.*, Observation of possible topological in-gap surface states in the Kondo insulator SmB_6 by photoemission, Nat. Commun. **4**, 3010 (2013).
[14] See Supplemental Material at http://link.aps.org/supplemental/10.1103/PhysRevB.99.245148 for more information regarding the experimental condition, basic principles, and additory analysis, which includes Refs. [17,20,22–26,29,30,37–39].
[15] C. H. Li, O. M. J. van 't Erve, J. T. Robinson, Y. Liu, L. Li, and B. T. Jonker, Electrical detection of charge-current-induced spin polarization due to spin-momentum locking in Bi_2Se_3, Nat. Nanotech. **9**, 218 (2014).
[16] A. Dankert, J. Geurs, M. V. Kamalakar, S. Charpentier, and S. P. Dash, Room temperature electrical detection of spin polarized currents in topological insulators, Nano Lett. **15**, 7976 (2015).
[17] J. F. Tian, I. Miotkowski, S. Hong, and Y. P. Chen, Electrical injection and detection of spin-polarized currents in topological insulator Bi_2Te_2Se, Sci. Rep. **5**, 14293 (2015).
[18] Y. Xia *et al.*, Observation of a large-gap topological-insulator class with a single Dirac cone on the surface, Nat. Phys. **5**, 398 (2009).
[19] S. Hong, V. Diep, S. Datta, and Y. P. Chen, Modeling potentiometric measurements in topological insulators including parallel channels, Phys. Rev. B **86**, 085131 (2012).
[20] S. Sayed, S. Hong, and S. Datta, Multi-terminal spin valve on channels with spin-momentum locking, Sci. Rep. **6**, 35658 (2016).
[21] C. H. Li, O. M. J. van 't Erve, S. Rajput, L. Li, and B. T. Jonker, Direct comparison of current-induced spin polarization in topological insulator Bi_2Se_3 and InAs Rashba states, Nat. Commun. **7**, 13518 (2016).
[22] C. Daboo, R. J. Hicken, E. Gu, M. Gester, S. J. Gray, D. E. P. Eley, E. Ahmad, J. A. C. Bland, R. Ploessl, and J. N. Chapman, Anisotropy and orientational dependence of magnetization reversal processes in epitaxial ferromagnetic thin-films, Phys. Rev. B **51**, 15964 (1995).
[23] W. C. Nunes, W. S. D. Folly, J. P. Sinnecker, and M. A. Novak, Temperature dependence of the coercive field in single-domain particle systems, Phys. Rev. B **70**, 014419 (2004).
[24] L. Q. Liu, A. Richardella, I. Garate, Y. Zhu, N. Samarth, and C. T. Chen, Spin-polarized tunneling study of spin-momentum locking in topological insulators, Phys. Rev. B **91**, 235437 (2015).
[25] D. J. Kim, T. Grant, and Z. Fisk, Limit Cycle and Anomalous Capacitance in the Kondo Insulator SmB_6, Phys. Rev. Lett. **109**, 096601 (2012).
[26] P. K. Li and I. Appelbaum, Interpreting current-induced spin polarization in topological insulator surface states, Phys. Rev. B **93**, 220404(R) (2016).
[27] E. Villamor, M. Isasa, L. E. Hueso, and F. Casanova, Temperature dependence of spin polarization in ferromagnetic metals using lateral spin valves, Phys. Rev. B **88**, 184411 (2013).
[28] E. K. de Vries, A. M. Kamerbeek, N. Koirala, M. Brahlek, M. Salehi, S. Oh, B. J. van Wees, and T. Banerjee, Towards the understanding of the origin of charge-current-induced spin voltage signals in the topological insulator Bi_2Se_3, Phys. Rev. B **92**, 201102(R) (2015).
[29] Z. J. Yue, X. L. Wang, D. L. Wang, J. Y. Wang, D. Culcer, and S. X. Dou, Crossover of Magnetoresistance from Fourfold to Twofold Symmetry in SmB_6 Single Crystal, a Topological Kondo Insulator, J. Phys. Soc. Jpn. **84**, 044717 (2015).
[30] F. Chen *et al.*, Magnetoresistance evidence of a surface state and a field-dependent insulating state in the Kondo insulator SmB_6, Phys. Rev. B **91**, 205133 (2015).
[31] D. Hsieh *et al.*, A tunable topological insulator in the spin helical Dirac transport regime, Nature (London) **460**, 1101 (2009).
[32] D. S. Kong *et al.*, Rapid surface oxidation as a source of surface degradation factor for Bi_2Se_3, ACS Nano **5**, 4698 (2011).
[33] D. Kim, S. Cho, N. P. Butch, P. Syers, K. Kirshenbaum, S. Adam, J. Paglione, and M. S. Fuhrer, Surface conduction of topological Dirac electrons in bulk insulating Bi_2Se_3, Nat. Phys. **8**, 459 (2012).
[34] J. F. Tian, S. M. Hong, I. Miotkowski, S. Datta, and Y. P. Chen, Observation of current-induced, long-lived persistent spin polarization in a topological insulator: A rechargeable spin battery, Sci. Adv. **3**, e1602531 (2017).
[35] J. S. Lee, A. Richardella, D. R. Hickey, K. A. Mkhoyan, and N. Samarth, Mapping the chemical potential dependence of current-induced spin polarization in a topological insulator, Phys. Rev. B **92**, 155312 (2015).
[36] M. Bianchi, D. D. Guan, S. N. Bao, J. L. Mi, B. B. Iversen, P. D. C. King, and P. Hofmann, Coexistence of the topological state and a two-dimensional electron gas on the surface of Bi_2Se_3, Nat. Commun. **1**, 128 (2010).
[37] Y. F. Li, Q. L. Ma, S. X. Huang, and C. L. Chien, Thin films of topological Kondo insulator candidate SmB_6: Strong spin-orbit torque without exclusive surface conduction, Sci. Adv. **4**, eaap8294 (2018).
[38] G. Li *et al.*, Two-dimensional Fermi surfaces in Kondo insulator SmB_6, Science **346**, 1208 (2014).
[39] J. C. Rojas Sánchez, L. Vila, G. Desfonds, S. Gambarelli, J. P. Attané, J. M. De Teresa, C. Magén, and A. Fert, Spin-to-charge conversion using Rashba coupling at the interface between non-magnetic materials, Nat. Commun. **4**, 2944 (2013).